PHYSICAL REVIEW A VOLUME 40, NUMBER 9 NOVEMBER 1, 1989

Collective effects in laser multiphoton ionization. II. Theoretical model and comparison with experimental results

F. Giammanco
Dipartimento di Fisica, Università di Pisa, Piazza Torricelli 2, 56100 Pisa, Italy
(Received 9 January 1989)

The time-space behavior of ions and electrons, whose density and temperature are typical of laser multiphoton-ionization experiments, is analyzed from the point of view of the fluid approximation taking into account all nonlinear terms. The analytic methods of solution, already presented, are applied to describe the three-dimensional coupled motion of both ions and electrons, including also the growth of charges during the laser pulse. The theoretical predictions are compared with the experimental results observed in a three-photon ionization experiment in Na, with special regard to the analysis of the electron current behavior as a function of the externally applied electric field.

I. INTRODUCTION

In the last years, little attention has been paid to the theoretical and experimental analysis of the time-space behavior of charges produced under typical conditions of ionization experiments in atomic physics. In fact, only recently several authors[1-8] who dealt with experiments devoted to study laser-matter interactions considered the importance of the generically called "space-charge" effects, but mostly as a problem that could modify the properties of ionized yields, as determined by the ionizing source.

In Ref. 9 it was demonstrated that the fluid approximation[10] is an appropriate approach to describing the time-space evolution of this class of plasmas. The basic equations that constitute this approximation are derived from the Boltzmann transport equation, such as the momenta of different order, averaged over an isotropic velocity distribution. Thus, those momenta describe the time-space evolution of the fluid mean quantities (velocity, density, energy) referred to in the laboratory frame. It was demonstrated that the fluid scheme holds true providing that the particle velocity, averaged over the distribution function, is equal to zero. Therefore, it is not strictly required that the distribution function approach the Maxwell distribution, as usually assumed. It turns out that the treatment can be extended to a wide class of experiments where the electron-electron equipartition time, depending on the charge density and on the electron temperature,[10] is longer than or comparable to the time scale of plasma evolution, i.e., above-threshold ionization (ATI) experiments. In fact, several authors[11-15] have measured the angular distribution of the ejected electrons as a function of the angle between the directions of the laser polarization and of the detection. The observed distribution is strongly peaked along the laser polarization and the sharpness increases as the order of the absorbed photons increases. In any case, along any axis there are two equiprobable opposite directions for the ejected electron velocity that assures a mean zero velocity.

This work presents an extension of the theoretical approach of Ref. 9. First of all, the method of solution is briefly recalled in order to point out the main features. Subsequently, it is demonstrated that the extension of the one-dimensional solution of coupled two-fluid motion to the three-dimensional case is straightforward at the same order of approximation.

Special attention is paid to the analysis of the production phase in order to take into account the influence of a finite production time on the growth of the self-generated electric field. It will be demonstrated that the inclusion of this term is not too difficult and does not imply a loss of information, providing that some hypotheses about the relative time scales of involved terms are verified.

In the last section the theoretical model is applied to explain the experimental results of Ref. 16, with special regard to the electron current behavior as a function of the external electric field. The dependences on the laser power of both ion yields and electron current are also analyzed in order to explain the observed deviations from ideal slope and to carry out the value of the charge threshold at which the collective effects become important.

II. THEORETICAL APPROACH

The fluid approximation describes the time-space evolution of the fluid mean quantities (velocity, density, and energy) referred to the laboratory frame. Since the macroscopic quantities are carried out by averaging over the velocity distribution function, it turns out that they are functions of coordinates and of time. The fluid velocity represents the common component of collective motion, whereas the temperature is related to the mean kinetic energy of random motion of particles. Thus, the energy conservation includes two terms which represent the internal energy of fluid function of temperature and the mean kinetic energy of collective motion related to fluid density and velocity.[10] If an isothermal expansion in vacuum is assumed, two partial differential equations, for fluid velocity and density, are sufficient to characterize the evolution, namely motion and continuity equations.[17]

The method of solution is introduced under assumption of negligible production time and an initial Gaussian-shaped profile of charges. In Sec. II B the internal self-generated electric field, which couples ion and electron fluid systems through the Poisson equation, is introduced. A solution is carried out by using, under suitable approximations, the same scheme used in the simplest case. Section II C deals with the problem of the production phase and its introduction in the previous solutions at the same order of approximation.

A. Single fluid

In the case of one-dimensional motion of a freely expanding fluid, neglecting both internal and external fields, the system to be solved is given by[10]

$$\frac{\partial v_j}{\partial t}+v_j\frac{\partial v_j}{\partial x}=-\left[\frac{kT_j}{m_j}\right]\frac{\partial}{\partial x}\ln(n_j)\ , \tag{1}$$

$$\frac{\partial n_j}{\partial t}+\frac{\partial}{\partial x}(n_j v_j)=0\ , \tag{2}$$

where v_j, n_j, m_j, and T_j are, respectively, velocity, density, mass, and temperature of the selected fluid. For monochromatic electrons, it is sufficient to introduce the electron energy in place of T_j, i.e., $kT=2E$.[9] If an initial Gaussian-shaped profile is assumed, the time-space evolution is represented by[9]

$$n_j(x,t)=n_0 f(t)^{1/2}\exp\left[-f(t)\left[\frac{x}{d}\right]^2\right]\ , \tag{3}$$

where $f(t)$ is a function of time. The fluid velocity v_j is related to $f(t)$ by means of the continuity equation [Eq. (2)]. In fact, dividing all terms by n_j, Eq. (2) is transformed in a first-order linear equation in x for the variable v_j, whose coefficients are time and space derivatives of $\ln(n_j)$, which immediately leads to the relation $v_j=-(x/2)D\ln[f(t)]$, where D represents the total time derivative. Introducing the equations giving the functional dependences on $f(t)$ of both v_j and n_j in the motion equation [Eq. (1)] and equating the terms with the same exponent of x, the second-order differential equation describing the time evolution of $f(t)$ is obtained, i.e.,

$$D^2 f(t)=\frac{3[Df(t)]^2}{2f(t)}-2B_j f(t)^2\ , \tag{4}$$

where $B_j=2kT/(m_j d^2)$. The initial conditions are $f(0)=1$ and $Df(t)|_{t=0}=0$. If $B_j t^2\gg 1$, $f(t)$ approximates the function $1/(1+B_j t^2)^{1.25}$.[9]

In the simplest case of constant or time-dependent (but independent on the space variable x) electric field, the solution of the single-particle-like equation $Dv_s=(e_j/m_j)E(t)$ must be added to the fluid velocity previously obtained, and the spatial variable must be replaced by $\int v_s dt-x$.

The extension of the solution method to describe the three-dimensional motion of a single fluid is straightforward owing to the independence of motion along the three axes. Moreover, the inclusion of momentum-exchange collisions with neutrals and time-varying temperature, or, in general, terms in the form $G(t)+F(t)x$, is very easy, only requiring modification in the differential equation of $f(t)$ and the single-particle-like one.[9]

B. Two-fluid coupled

According to the above method of solution, it is possible to analyze, although in an approximate way, the motion of electrons and ions coupled with the self-generated electric field. The system to be solved is now represented through five partial differential equations including two motion equations, coupled by the internal field, two continuity equations, and the Poisson equation, which relates the internal self-generated field to the ion and electron densities.[10] In Ref. 9 by restricting the treatment to the one-dimensional case and assuming Gaussian shapes such as Eq. (3) for ions and electrons, a solution was carried out by linearizing the Poisson equation. In the one-dimensional case the electric field is given by the integral

$$E_\rho(x,t)=4\pi e\,dn_0\int_{\epsilon_i}^{\epsilon_e}e^{-\epsilon^2}d\epsilon\ , \tag{5}$$

where the variable change $\epsilon_j=f_j^{1/2}(x_{sj}-x)/d$ has been introduced. The index j refers to both species, and the other symbols are already defined. By series integration and retaining the first term, the following is immediately obtained:

$$E_\rho(x,t)=4\pi e n_0[f_i^{1/2}(x-x_{si})-f_e^{1/2}(x-x_{se})]\ . \tag{6}$$

Equation (6) is valid insofar as the second term of series development is negligible. Thus, the spatial limit of validity of the previous solution is given by the condition

$$\epsilon_e-\epsilon_i\geq(\epsilon_e^3-\epsilon_i^3)/3\ . \tag{7}$$

Introducing the internal field given by Eq. (6) in the coupled system and equating terms with the same exponent of x, the differential equations describing the coupled evolution of $f_j(t)$ and $x_{sj}(t)$ are given by

$$D^2 f_j=\frac{3(Df_j)^2}{2f_j}-2B_j f_j^2\pm 2\omega_{pj}^2 f_j(f_i^{1/2}-f_e^{1/2})\ , \tag{8}$$

$$D^2 x_{sj}=\frac{e_j}{m_j}E_0\pm\omega_{pj}^2 f_{j^a}^{1/2}(x_{si}-x_{se})\ , \tag{9}$$

where the upper sign refers to the electrons and $\omega_{pj}=4\pi e^2 n_0/m_j$ is the plasma frequency. The symbol j^a denotes that if x_{sj} refers to ions, f_j refers to electrons and vice versa. In Eq. (9) an external field E_0 has been also introduced. In fact, owing to the initial conditions $x_{sj}(0)=0$ and $Dx_{sj}(0)=0$, Eq. (9) gives a nontrivial solution only in the presence of an external field.

A numerical test has been performed in order to verify the limit of validity of the approximations in a range of variation of the involved parameters (density, temperature, initial shape, and so on) typical of ionization experiments in atomic physics. Figure 1 shows, as an example, the spatial profile of the electron density at the time instant $t=100$ ns (electron density of 10^{11} electrons/cm^3,

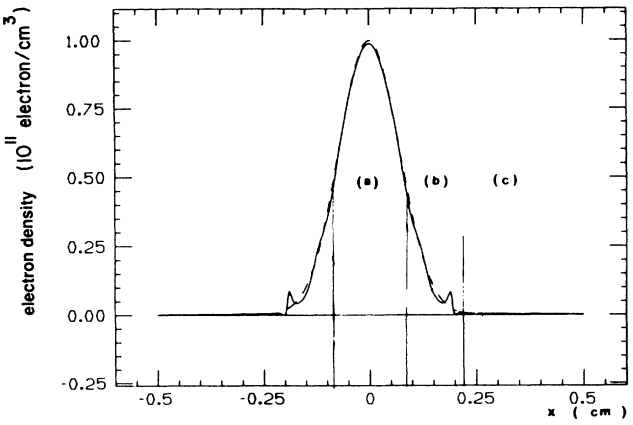

FIG. 1. Spatial profile of electron density at $t=100$ ns. Charge density 10^{11} electrons/cm^3. Solid line represents the solution by using a finite difference numerical code. Dashed line: spatial profile as deduced from the solution of Eqs. (15) and (16). (a) Strongly coupled region ($\omega_{pj}\neq 0$); (b) transition region; (c) free expansion ($\omega_{pj}=0$).

electron temperature of 1 eV, and $E_0=0$) deduced by numerical integration of the complete two-fluid one-dimensional coupled system and by the solution of Eqs. (8) and (9) (dashed line). The model describes electron and ion motion in the region (a) of Fig. 1, whose width is about the half width of the Gaussian profile well. Region (c) is in agreement with the single-fluid solution, obtained by Eqs. (8) and (9) with $\omega_{pj}=0$. The area of region (c) represents the number of electrons leaving the interaction volume. The transition region (b) is very thin and exhibits unstable numerical evolution. The observed sharp peak occurs when the collective fluid velocity is approximately equal to the thermal velocity that corresponds to the first instants of the shock wave growth.[17] Thus, in this sharp region the previous assumption of collisionless isothermal expansion does not hold and a different approach, including energy conservation and electron-ion collisions is required.[17] The contribution of region (b) is small in terms of the total number of involved charges. Hence, the spatial limit of validity of the obtained solution deduced from Eq. (7) can be assumed being a sharp boundary between coupled and single-fluid behavior.

The absolute value of charges leaving the coupled zone is a function of time as a consequence of Eq. (7). Representing the solution in the region of free expansion by

$$n_f = k(t) f(t)^{1/2} \exp[-f(t)(x/d)^2] , \tag{10}$$

where the evolution of the $f(t)$ function is described by Eqs. (8) and (9), with $\omega_{pj}=0$, $k(t)$ is given by the mass conservation, i.e.,

$$n_0 2\int_0^{\epsilon^*} e^{-\epsilon^2} d\epsilon + k(t) 2\int_{\epsilon^*}^{\infty} e^{-\epsilon^2} d\epsilon = \sqrt{\pi} dn_0 , \tag{11}$$

where ϵ^* is a value that satisfies the condition (7). The first integral is calculated by introducing the value of $f(t)$ given by the coupled system, whereas in the second integral the $f(t)$ value is the solution with $\omega_{pj}=0$. The shape of the solution for fluid velocity and density and the supporting equations is not modified by the introduction of the $k(t)$ function.

The three-dimensional extension of the previous solution is straightforward by using a similar linearization of the Poisson equation. Assuming an external field directed along the x axis, the components of the internal field are now given by

$$E_{\rho x}(x,t) = \tfrac{4}{3}\pi e n_0 [(f_x f_y f_z)_i^{1/2}(x - x_{si}) - (f_x f_y f_z)_e^{1/2}(x - x_{se})] , \tag{12}$$

$$E_{\rho y}(y,t) = \tfrac{4}{3}\pi e n_0 [(f_x f_y f_z)_i^{1/2} - (f_x f_y f_z)_e^{1/2}]_y , \tag{13}$$

$$E_{\rho z}(z,t) = \tfrac{4}{3}\pi e n_0 [(f_x f_y f_z)_i^{1/2} - (f_x f_y f_z)_e^{1/2}]z . \tag{14}$$

Three equations like Eq. (7) will give the limits of validity of the coupled solution along the three axes, provided that the appropriate $f(t)$ and initial width d are introduced. Hence, the system to be solved becomes

$$D^2 f_{k,j} = \frac{3(Df_{k,j})^2}{2f_{k,j}} - 2B_{k,j} f_{k,j}^2 \pm (\tfrac{2}{3})\omega_{pj}^2 f_{k,j} [(f_x f_y f_z)_i^{1/2} - (f_x f_y f_z)_e^{1/2}] , \tag{15}$$

$$D^2 x_{sj} = \frac{e_j}{m_j} E_0 \pm \tfrac{1}{3}\omega_{pj}^2 (f_x f_y f_z)_j^{a\,1/2}(x_{si} - x_{se}) . \tag{16}$$

The index j refers to the species and the index k to the coordinate. Note that the $f(t)$ time evolution, along any axis, depends essentially on the parameter B, that is on the width of the initial profile.

C. Production phase

In the above solution, the initial profile of charges is supposed to be produced in a time negligible compared with the fluid evolution. In many experiments, this assumption does not imply any loss of generality, owing to the different scale between production and collection time. On the contrary, the scheme of the experiment of Ref. 16 does not allow such an approximation especially with regard to the electrons, whose collection time is comparable with the laser pulse duration (≈ 10 ns).

In general, the introduction of rate terms in the continuity equation does not make the previous solution scheme valid, and, particularly, the assumption of self-similar expansion of the initial profile. Thus, separation of spatial and temporal dependences is not allowed. Nevertheless, depending on the relative time scales of involved terms, the production phase can be introduced in the previous scheme at a degree of approximation of the same order as that used in linearizing the Poisson equation. In general, if the time scale of expansion is greater than the production time, the term representing the flux of particles $[\nabla(nv)]$ can be neglected compared with the density time derivative. Therefore, the continuity equation is reduced to the usual rate equation admitting separation of variables if the source term can be expressed as a product of two separated functions of coordinates and time. In the experimental conditions of Ref. 16 during

the laser pulse (10 ns), ions are at rest. In fact, the time scale of ion collection is some μs, in the investigated range of external electric field values (3–100 V/cm). As a consequence, the evolution of the ion density is represented by $g(t)n_p(x,y,z,t)$, where n_p is given by Eq. (3) or Eq. (11), according to Eq. (7), and $g(t)$ is the solution of the rate equation

$$\frac{dg(t)}{dt}=\langle a\rangle I_L^{\alpha}(x,y,z,t)[N-g(t)] . \tag{17}$$

In Eq. (17), N represents the unperturbed beam density and $\langle a\rangle$ the ionization cross section. $I_L(x,y,z,t)$ is the laser intensity that may be expressed as a product of two independent functions of space and time, and α is the order of the transition that is the number of photons required to overcome the ionization potential. It has been also assumed that only ions and neutral atoms, in the fundamental state, are present in the beam. However, more complex rate equations involving different excited species are allowed, under the condition that those processes occur in a time shorter than the time scale of motion.

The new solution requires only a few modifications of the system describing the ion motion. In fact, it is sufficient to introduce $g(t)$ given by Eq. (17) in place of the initial density n_0 in the plasma frequency. The functional dependence of the fluid velocity on $f(t)$ and on spatial variables is unaffected by the introduction of $g(t)$, because only the gradient of the logarithmic density appears in the motion equation.

Owing to the different time scale of expansion, the behavior of electrons cannot be described in as simple a way as the ion one, if detailed information about the time-space profile is required. Nevertheless, since the constitutive equations of fluid description represent the mean time-space evolution of the macroscopic quantities, it seems worth introducing the electron behavior in such a way that the basic scheme of analysis requires only a few modifications.

The relevant time scales to be considered, with regard to the electron evolution, are related to the plasma frequency growth during the production phase, proportional to the $g(t)$ function [Eq. (17)] and to the density gradient through the coefficient B.

If the condition $\omega_{pe}^2(t)[1-(f_xf_yf_z)_e^{1/2}]\gg B_ef_e$ is verified in the first instant of the interaction, electrons are strongly coupled with ions and their $f_e(t)$ function differs from 1 (the ions are at rest) approximately for a factor $B_e/\omega_{pe}^2(t)$. In this case, the coupling term is simply given by

$$\omega_{pj}^2 g(t)f_j[(f_xf_yf_z)_i^{1/2}-(f_xf_yf_z)_e^{1/2}] , \tag{18}$$

where the $g(t)$ function has been normalized to the gas density N and $\omega_{pj}^2=(4\pi e^2/m_j)N$.

The opposite condition, that is, when the electrons leave the interaction zone as soon as they are produced, implies that the term depending on $f_e(t)$ in Eq. (18) can be neglected compared with the corresponding ion functions. Finally, in an intermediate condition, the production time can be divided in time intervals, whose duration τ must satisfy the relation $\tau B_e^{1/2}\ll 1$. Therefore, the electrons produced during each time interval of τ duration are in a good approximation at rest. The system describing the total evolution of electrons is constituted by a set of coupled equations equal to the number of intervals into which the production time is divided. The differential equation referred to the $f_{n,e}(t)$ function of electrons produced in a time $n\tau<t<(n+1)\tau$ includes common terms depending on the ion electric field, namely $\omega_{pe}^2 g(t)f_{n,e}(f_xf_yf_z)_i^{1/2}$, and terms related to the evolution of electrons produced in the previous time intervals, i.e.,

$$\omega_{pe}^2 g(\tau)f_{n,e}(f_xf_yf_z)_{1,e}^{1/2}+\omega_{pe}^2[g(2\tau)-g(\tau)]f_{n,e}(f_xf_yf_z)_{2,e}^{1/2}+\cdots+\omega_{pe}^2[g(t-n\tau)-g(n\tau)]f_{n,e}(f_xf_yf_z)_{n,e}^{1/2} . \tag{19}$$

The initial conditions for the differential equation representing the time evolution of $f_{n,e}$ are $f_{n,e}(t=n\tau)=1$ and $Df_{n,e}|_{t=n\tau}=0$.

The approximation of Eq. (19), although useful to maintaining the method of solution, introduces a serious increase of calculation time. Fortunately, $f_e(t)$ decreases, in the first instants, no so fast[9] as it could be deduced by assuming the asymptotic formula of Eq. (4). Moreover, in the conditions of a wide class of experiments, and especially in case of nanosecond pulsed-laser sources, the simple coupling term of Eq. (18) leads, at the end of the ionization interaction, to results comparable to those obtained by using a system of n differential equations, providing that an effective width be introduced, namely,

$$d_{\text{eff}}=(kT_e/m_e)^{1/2}\tau_L , \tag{20}$$

where τ_L is the laser pulse duration. Equation (20) represents the increase of volume occupied by electrons during the laser pulse.

III. COMPARISON WITH EXPERIMENTAL RESULTS

In this section the model is applied to describing the results of Ref. 16 with special regard to the electron current versus the external electric field. The peak dependences of electron current and ion yields on the laser intensity are analyzed with the aim of determining the charge threshold. Thus, the electron current and ion peak dependences on the laser intensity are compared with an ideal multiphoton (MPI) slope at the same experimental values of beam density (1.610^{11}, 2.710^{11}, and 4.410^{11} atoms/cm^3). The variation of the ion time of flight, as a function of the laser intensity, is also com-

pared with the experimental dependence.[16]

If volume effects are neglected, a noticeable simplification occurs for the supporting differential equation system to be solved. In fact, assuming a spherical symmetry, only one equation for each species, like Eq. (15), is required to describe the charge evolution in the coupled zone. Equation (15) for ions and electrons must be solved also with $\omega_{pj}=0$, in order to carry out, by using Eq. (10), the total number of charges in both zones. In the experimental conditions of Ref. 16, the time scales of production phase, thermal expansion, and collection time are quite similar, i.e., about 10 ns. In fact, typical values are ≈ 1 eV for the electron temperature, ≈ 0.01 cm for the focussing spot, ≈ 14 V/cm for the external electron field, and 3 cm for the distance of plate-collecting electrons.[16]

According to Sec. II C, the coupling term is given by Eq. (18), width an effective width deduced from Eq. (20), i.e, ≈ 0.1 cm. A test performed by using a set of ten equations, including terms like Eqs. (19), did not show important differences.

The electron current on the plate surface, whose radius is R at a fixed position A, is obtained by integrating the component of current along the direction of the field (orthogonal to the laser direction) on the radial variable that leads to

$$I_T \propto Ng(t)v_{xe}[f(t)]_e^{1/2}\exp\left[-\frac{[f(t)]_e}{d^2}(x_{se}-A)^2\right] \times\left[1-\exp\left[-\frac{[f(t)]_e}{d^2}R^2\right]\right], \quad (21)$$

where v_{xe} is given by

$$v_{xe}=v_{se}+0.5(x_{se}-A)D\ln[f_e(t)] .$$

d is the initial half width of the profil, $g(t)$ is obtained as the solution of the rate equation, and N is the beam density.

In the form of Eq. (21), the current is referred to the coupled zone. Thus, $f(t)$, given by the solution of the coupled set of equations, must satisfy the condition of Eq. (7), at the position A of the detector. On the opposite condition, the total current is given by the same equation, but $f(t)$ is deduced from the uncoupled system, with $\omega_{pj}=0$, and the charge density $[Ng(t)]$ must be multiplied by $k(t)$, given by Eq. (11).

The total number of ions, collected at a detector position A_1, whose diameter is R_1, is immediately carried out, i.e.,

$$N_{\text{ion}} \propto Ng(t)[f(t)]_i^{1/2}\exp\left[-\frac{[f(t)]_i}{d^2}(x_{si}-A_1)^2\right] \times\left[1-\exp\left[-\frac{[f(t)]_i}{d^2}R_1^2\right]\right] . \quad (22)$$

If the plasma frequency is negligible compared with the B value, both coupled and uncoupled solutions overlap and only one peak of current is observed, whose arrival time is approximately equal to that of a single particle uniformly accelerated by the external field. A simple derivation of the electron-current dependence on the electric field can be carried out by using the asymptotic expression of $f(t)$ given in the Sec. II A (single fluid). Assuming that collection time and velocity exhibit the single-particle dependences on the electric field, respectively, $E_0^{1/2}$ and $E_0^{-1/2}$, the f value at the position A of the detector is represented by $f \approx E_0^{1.25}/(E_0+2BAm/e)^{1.25}$. If $E_0 \gg 2BAm/e$, i.e., in the experimental conditions of Ref. 16 $E_0 \gg 600$ V/cm, the density profile simply translates, and, thus, the peak of current dependence is just $E_0^{1/2}$. Owing to the variation range of the applied external field (4–100 V/cm) (Ref. 16) the opposite condition holds true. If the argument of the exponential function containing the ratio between the radius of the detector and the half width of the initial profile is $\ll 1$ [Eq. (21)], the peak of current is proportional to $f^{3/2}E^{1/2}$, which leads to the dependence $E^{2.375}$, whereas in the opposite condition the dependence is $E^{1.125}$. Referring to the experimental results presented in Fig. 2 (dots) (see also for further details Fig. 11 of Ref. 16), the fast 1 and 0.1-mJ peaks both exhibit, below 20 V/cm, a slope ≈ 2, which means the argument of the exponential in Eq. (21) is <1, i.e., the profile of untrapped electrons does not expand out of the detector surface. The solid lines represent the behavior as deduced from the complete solution of the system with a charge density of 10^{10} electrons/cm^3 for 1-mJ peaks and 10^8 electrons/cm^3 for 0.1-mJ peaks. The ratio between fast and slow 1-mJ peak depends on the numerical condition Eq. (7) must fulfill. In fact, the absolute value of charge density in the coupled and freely expanding zones is just a function of that limit, entering the integral Eq. (11). The experimentally observed ratio of peaks is reproduced by equating the terms of Eq. (7). It turns out that the transition zone (c) (see Fig. 1) gives a contribution, in terms of

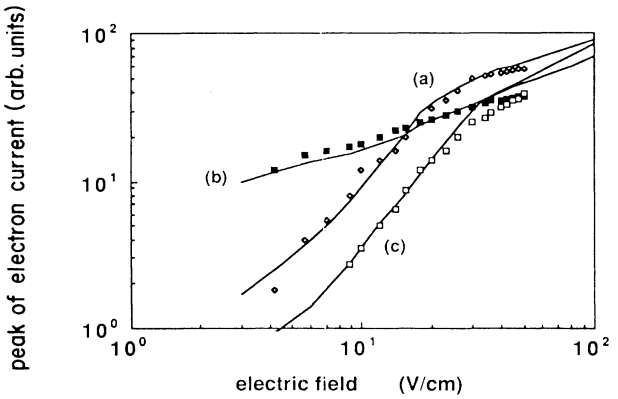

FIG. 2. Peak of the electron current vs externally applied electric field. The dots represent the experimental results of Ref. 16. Laser focussed by short focus lens, $\lambda=5787$ Å. Beam density 4.4×10^{11} atoms/cm^3. (a) and (b) The observed peaks at a laser intensity of 200 MW/cm^2; (c) the peak at 20 MW/cm^2. Solid lines represent the theoretical calculations. Charge density 10^{10} electrons/cm^3 for peaks (a) and (b) and 10^8 electrons/cm^3 for peak (c).

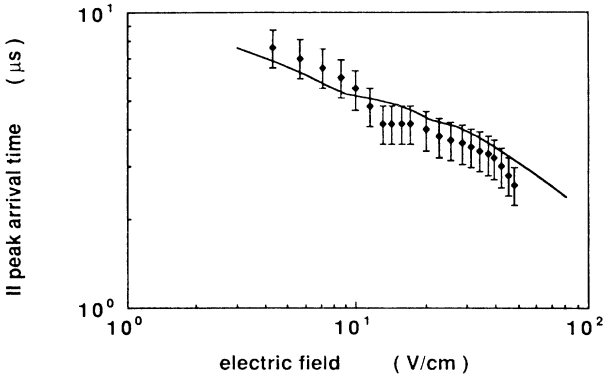

FIG. 3. Arrival time of slow peak vs externally applied electric field. Same experimental conditions of Fig. 2. Solid line: theoretical calculations.

particle trapping, represented well by a spatial extension of the zone, where the linearization of the Poisson equation holds true.

Figure 3 shows the theoretical dependence of arrival time of slow 1-mJ peak. The theoretical slops of both arrival time and peak of current are close to the $E^{-1/2}$ and $E^{1/2}$ single-particle dependences. The superimposed modulation, also observed in the experimental results, can be ascribed to an additional oscillation arising from the condition of Eq. (7), and, hence, from the $k(t)$ function. However, the spread of the slow-peak profile does not allow an improvement in the resolution. In fact, the error bars do not depend on instrumental resolution, but on the real width of the peak (see Fig. 13 of Ref. 16).

Figures 4, 5, and 6 are related to some features observed in the dependence on the laser intensity. Figure 4 shows the increase of the ion time of flight as laser intensity increases as observed in Ref. 16 by using a short focus lens. In the theoretical calculations, it has been assumed a three-photon transition and a value of the ionization cross section in such a way that the range of produced charges is similar to that approximately deduced from the experimental measurements, i.e., 10^8–10^{10} electrons/cm^3. The error bars depend on a not-too-sharp definition of the peak, probably due to a residual volume effect in the caustic of the lens.

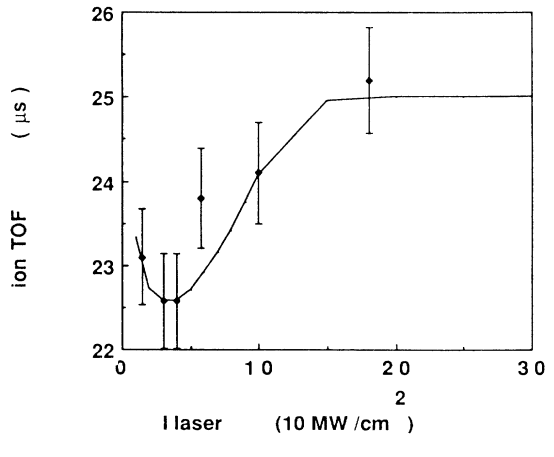

FIG. 4. Ion peak time of flight (TOF) vs laser intensity. Beam density 4.4×10^{11} atoms/cm^3. Charge density$=10^{10}$ electrons/cm^3; $\lambda=5787$ Å. The dependence on laser intensity is given in Fig. 10, Ref. 16. Solid line: theoretical calculations.

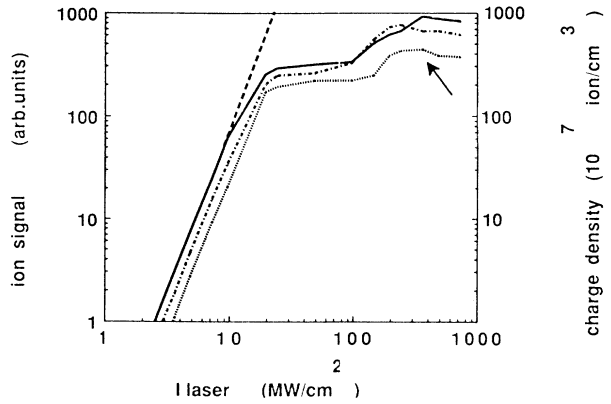

FIG. 5. Theoretical dependence of the ion signal vs laser intensity for a three-photon transition for the atomic densities: 1.6×10^{11}, 2.7×10^{11}, and 4.4×10^{11} atoms/cm^3 from bottom to top. Dashed line: growth of charge density in the absence of collective interactions. Right scale shows the value of produced charge density. Arrow refers to the total ionization of gas.

Finally, as an example, Figs. 5 and 6 show the ion signal and electron current peak as a function of the laser intensity compared with an ideal three-photon transition, for three different initial beam densities (1.6×10^{11}, 2.7×10^{11}, and 4.4×10^{11} atoms/cm^3). The ion slopes deviate from the ideal one (dashed line) at about the same value of produced charges, regardless of the initial beam density. The slopes of Fig. 5 are quite similar to those experimentally observed.[16] In particular, Fig. 5 must be

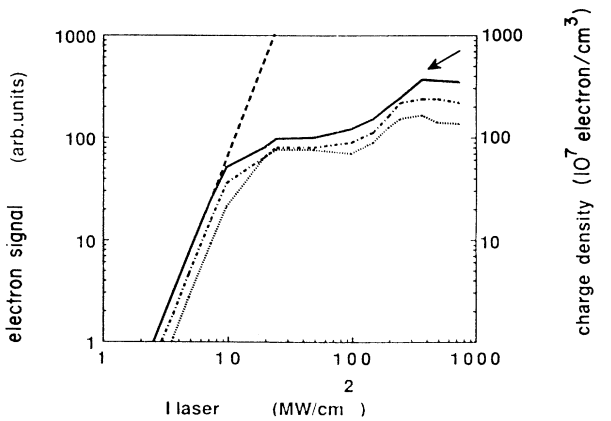

FIG. 6. Peak of electron current vs laser intensity. Theoretical slopes. Same conditions of Fig. 5.

compared with the signal of ions coming from the spot size. Referring to Figs. 5 and 6 of Ref. 16, when the slope of ions produced in the focus of the lens saturates, the signal due to ions coming from outer zones at a lower level of charge density still grows according to slope three.

The dependence of the electron current (Fig. 6) shows the same characteristics. In this case, a direct comparison with the measured behavior is complicated by the poor time resolution of the detection technique that leads to a mixing of contributions from zones at a different charge density. Thus, deviations from the ideal slope due to the collective effects in the spot size could be partially attenuated by the overlapping of signals coming from outer zones. In any case, the absolute value of charge threshold, for electrons and ions is close to the measured one.

A simple estimation of the charge density threshold can be obtained from Eq. (15). As the charge density increases, the coupling term, depending on the electronic plasma frequency, inhibits the expansion associated to the thermal motion ($B_e f_e^2$). The electronic profile oscillates around the ionic one, with an amplitude approximately given by dB_e/ω_{pe}^2.[9] In the regime of strong coupling, that amplitude must be ≤ 1, i.e.,

$$n_e \geq \frac{2kT_e}{4\pi e^2 d^2} \ . \tag{23}$$

Equation (23) can be also obtained from the neutrality condition implying a Debye length smaller than the plasma characteristic length.[10] By introducing previous values, Eq. (23) gives $n_e \geq 3.10^8$ electrons/cm^3, in agreement with the results of numerical calculations (Fig. 6) and with the experimental estimation. The ion signal exhibits a similar threshold behavior with a plateau reached at a produced charge density roughly 10 times larger than the electron one.[16] In fact, the expansion of the ion profile is enhanced by an energy transfer from electrons to ions, and larger ionic charge density can be expected to reach the plateau. In this case, terms in Eq. (15) related to the ionic plasma frequency and to the square derivative play a dominant role. Thus, the threshold value for ions can be carried out only by numerical calculations.

The anomalous saturation value can explain the variation of ratio between atomic and molecular ions as a function of laser power. In fact, whereas the change in slope of the atomic ion signal occurs at a charge density of $\approx 10^{10}$ ion/cm^3, the molecular ion one can be ascribed to total ionization of molecules in the beam. It turns out, from Figs. 4, 5, and 6 of Ref. 16, an initial concentration of $\approx 5.10^9$ mol/cm^3, a value close to the thermal equilibrium one.

IV. CONCLUSIONS

The quite satisfactory results of the theoretical model in explaining the main features of the experimental ion and electron behaviors suggests that the approach, although approximated, gives a good quantitative description of the time-space evolution of charges produced in typical MPI experiments, provided that a specific diagnostic is added to the standard MPI apparata. In fact, the quantitative comparison with experiments depends on the numerical condition that Eq. (7) must fulfill, whose value can be carried out only by specific measurements. Particularly, in the experiment of Ref. 16, the numerical condition was deduced from the ratio of electron current slow and fast peaks versus the external field.

The anomalous value of saturation of MPI slope shows that the cross section of process cannot be determined simply by assuming that the change in slope corresponds to the total ionization of gas, i.e., $\langle a \rangle I_S^{\alpha} = N$, where α is the order of transition, N the gas density, and I_S the saturation intensity. For instance, in the present experiment, the cross section would be overestimated, in case of ions, for a factor 3.5, taking into account a charge threshold value of $\approx 10^{10}$ ion/cm^3, and for a factor 7.4 in case of electrons (threshold $\approx 10^9$ electrons/cm^3). Thus, the wide spread of cross-section values, as deduced from literature, especially referred to alkali vapors, could be explained as an interference between purely collisional processes and collective plasma interactions, whose influence is strongly dependent on the specific experimental conditions, i.e., charge densities, applied electric field, and so on.[18]

Recently, several authors reported experimental evidence of phenomena, apparently different from each other, as chaotic evolution of electric discharge,[19]) bistable transmission of laser light[20] through a cell containing Na and buffer gas, and electron and ion focussing in electron-atom impact ionization.[21,22] Authors underlined the essential role of plasma interactions in order to describe the observed phenomena. Particularly in Refs. 21 and 22, a very complex spectrum of high-frequency plasma "electrostatic" oscillations was recorded in a correspondence to relevant focussing effects, ascribed to interactions between a self-generated electric field of produced charges and electron beam. In the framework of Eqs. (15), a time-evolving frequency spectrum, determined by the "beats" among the variable in time frequencies of electrons and ions and by the anharmonicity of motion due to the gradient pressure terms, can be predicted.

The experiment of Ref. 20, although performed by using cw laser, is an example of interference between short-range collisions and plasma motion. In fact, according to the explanation given by the authors, at the first instants, the plasma production is assisted by collisions between atoms excited by laser radiation, but the subsequent evolution, and, hence, the absorption of radiation, is strongly coupled with the plasma properties (diffusional motion, recombination, ionization from high-lying levels, and so on[23]).

The growth of interest around this class of plasmas and related atomic phenomena encourages improvement of the above-described method of analysis, in view of its relative simplicity and the quite satisfactory agreement with the experiment.

A description of the transition region between coupled and freely expanding evolution seems important in order to analyze the chaotic features of the discharges.[19] In fact, as above underlined, the numerical instability is re-

lated to the physical phenomenon of shock-wave growth, which requires inclusion of dissipative terms in the basic equations, and simultaneous solution of the energy conservation, to take into account transfer between internal (random motion) and collective energy.[10,17] However, the obtained solutions can be considered as a guide for the overall solution, those representing the time-space evolution of the central zone and of the tails of the charge profile.

[1]M. Crance, J. Phys. B **19**, L267 (1986).
[2]F. Yeargeau, G. Petite, and P. Agostini, J. Phys. B **19**, L663 (1986).
[3]G. Petite, P. Agostini, and F. Yeargeau, J. Opt. Soc. Am. B **4**, 765 (1987).
[4]L. A. Lompré, A. L'Huillier, G. Mainfray, and C. Manus, J. Opt. Soc. Am. B **2**, 1906 (1985).
[5]P. Kruit, J. Kimman, H. G. Muller, and M. J. van der Wiel, Phys. Rev. A **28**, 248 (1983).
[6]P. H. Bucksbaum, M. Bashkansky, R. R. Freeman, T. J. McIlrath, Phys. Rev. Lett. **56**, 24 (1986).
[7]T. J. McIlrath, P. H. Bucksbaum, R. R. Freeman, and M. Bashkansky, Phys. Rev. A **35**, 4611 (1987).
[8]For a review of the influence of space-charge phenomena in different fields of investigation and mostly application see *Resonance Ionization Spectroscopy III*, edited by G. S. Hurst (Hilger, Bristol, United Kingdom, 1987) and *Resonance Ionization Spectroscopy IV*, edited by T. B. Lucatorto and J. E. Parks (Hilger, Bristol, United Kingdom, 1988).
[9]F. Giammanco, Phys. Rev. A **36**, 5658 (1987).
[10]L. Spitzer, *Physics of Fully Ionized Gases* (Interscience, New York, 1956); L. D. Landau and E. M. Lifshitz, *Kinetic Physics* (Mir, Moscow, 1979).
[11]G. Leuchs, J. Reif, and H. Walter, J. Appl. Phys. B **28**, 87 (1982).
[12]H. J. Humpert, H. Schwier, R. Hippler, and H. O. Lutz, Phys. Rev. A **32**, 3787 (1985).
[13]A. Dodhy, R. N. Compton, and J. A. D. Stckdale, Phys. Rev. Lett. **54**, 5 (1985).
[14]F. Fabre, P. Agostini, G. Petite, and M. Clement, J. Phys. B **14**, L677 (1981).
[15]G. Petite, F. Fabre, P. Agostini, M. Crance, and M. Aymar, Phys. Rev. A **29**, 2677 (1984).
[16]F. Giammanco, Phys. Rev. A **40**, 5160 (1989) (preceding paper).
[17]Ya. B. Zel'dovich and Yu. P. Raizer, *Physics of Shock Waves and High Temperature Hydrodynamic Phenomena* (Academic, New York, 1966).
[18]E. Arimondo, F. Giammanco, A. Sasso, and M. I. Schisano, Opt. Commun. **55**, 329 (1985).
[19]P. Y. Cheung and A. Y. Wong, Phys. Rev. Lett. **59**, 551 (1987).
[20]P. Verkerk and G. Grynberg, Europhys. Lett. **6**, 31 (1988).
[21]G. I. Guseva and M. A. Zav'yalov, Fiz. Plazmy **9**, 770 (1983) [Sov. J. Plasma Phys. **9**, 445 (1983)].
[22]V. P. Kovalenko and S. F. Fastovets, Fiz. Plazmy **9**, 964 (1983) [Sov. J. Plasma Phys. **9**, 562 (1983)].
[23]F. Giammanco and S. Gozzini, Nuovo Cimento B **66**, 1 (1981).